PFC/JA-82-17

HIGH RESOLUTION X-RAY SPECTROSCOPY FOR DIAGNOSTICS OF SINGLE TOKAMAK DISCHARGES

E. Källne and J. Källne

Plasma Fusion Center
Massachusetts Institute of Technology
Cambridge, MA 02139

August 1982

This work was supported by the U.S. Department of Energy Contract No. DE-AC02-78ET51013. Reproduction, translation, publication, use and disposal, in whole or in part by or for the United States government is permitted.

High Resolution X-ray Spectroscopy for Diagnostics of Single Tokamak Discharges

E. Källne and J. Källne

Harvard-Smithsonian Astrophysical Observatory

Cambridge, Massachusetts 02138, USA

Abstract

We report on an experiment which has been used to measure soft X-ray line emission spectra from highly charged impurity elements in the hot plasma of the Alcator C tokamak. These measurements shall serve as a diagnostic of plasma parameters; the temperature (of ions and electrons), the electron and impurity ion densities, and charge state distributions. Results from the initial measurements of the He- and H-like spectra of S and Cl are presented as well as spectra from molybdenum in charge states between Mo^{28+} and Mo^{32+}. Dependencies of the measured spectra on plasma parameters are provided. The aim of this experiment is to conduct broad-band time-resolved spectroscopic diagnosis of tokamak plasmas. To this end we discuss pertinent requirements of spectrometer performance and the development of a new position sensitive X-ray detector system.

I. Introduction

X-ray spectroscopy has lately experienced a renaissance since it has been called upon to serve as a diagnostic tool of hot plasmas by analyzing emission from highly charged ions. This has meant that X-ray spectroscopy has become an important part of presently very actively pursued research areas such as X-ray astronomy [1], and fusion energy research [2]. These ions exist in a plasma in a state of steady conditions, specifiably in thermal (coronal) equilibrium or in some state of departure therefrom, and can provide information complimentary to that of heavy ion collision reactions [3]. The diagnostic is based on the characteristic emission spectra of highly ionized atoms. The foundation for the interpretation and analysis of spectra from plasmas was developed some forty years ago through the classical work on spark generated plasmas by Edlén and co-workers [4]. The present day light sources come in many different shapes and various packages, and instrumentation for X-ray spectroscopic diagnostics must be designed with regard to the particular application. Moreover the measurements to be done are dictated by the kind of diagnostics information required. We have built up an experiment at the Alcator C tokamak at MIT [5] to perform high resolution X-ray line emission measurements in the wavelength region 4.3-5.3 Å or 2.4-2.7 keV. We shall describe the salient features of this experiment, discuss some pertinent aspects of the plasma and present results from the first phase of this project.

In the present experiment, the objective was to develop a versatile tokamak X-ray spectroscopy diagnostic (TOXRASD). The X-ray emission stems from small amounts of impurity elements in plasmas of hydrogen, deuterium, or helium. The impurity concentration in the Alcator tokamak is usually kept very low (with Z_{eff} typically 1.1-1.5), which is achieved by cooling

the walls [6]. Needless to say, this is not aimed so much towards optimization for TOXRASD measurements as it is a step to reach the conditions for plasma fusion. However, using a spectrometer with high light collection efficiency, good quality X-ray spectra can be recorded, even for trace element concentrations for individual plasma discharges. The Alcator machine produces plasmas in the temperature range one to two keV and density range of (0.5-8) x $10^{14}cm^{-3}$. Therefore, low Z elements (Z<10 of which C, N, and O are found in Alcator) in the central core of the plasma are fully stripped of the electrons while medium Z elements (for instance Al, S, Cl, Cr, and Fe) appear as few electron ions. In the λ-range 4.3-5.3 Å we find radiation from $S^{13+,14+,15+}$ and $Cl^{14+,15+}$. The high Z element (Z=42) molybdenum (the limiter material) is also found in the charge states 28+ to 32+.

The few electron systems are of particular interest because of their relatively simple level structure which in turn simplifies both measurement and interpretation. Furthermore, these ions have relatively high ionization potential gaps, and remain radiating from the plasma for extended periods of time up to the limit of the confinement time of the plasma which is about 30 ms for Alcator C [5]. A plasma discharge is maintained in a steady state condition for 100 to 200 ms, which is a long time period on the scale of typical atomic relaxation times. The spatial distributions of the few electron ions are fairly constant over the plasma core region where the electron temperature remains constant [7]. H- and He-like spectra are therefore attractive for TOXRASD over quite a range of energies. These spectra consist of well separated lines of small natural widths so the Doppler broadening from ion temperatures of 1 to 2 keV is a noticeable contributor to the line profile, if measured at a resolution of

$\Delta E/E < 1/3000$. Furthermore, the line intensities of the characteristic emission reflect population rates of the excited atomic states involved, which in turn depend on the prevailing plasma conditions including electron temperature (T_e), electron density (n_e), etc. [8]. Part of TOXRASD are therefore theoretical calculations which express the dependence of certain line ratios on the main plasma parameters [9]. Our measurements relate to n=2 to n=1 X-ray transitions of the He-like spectrum for S and Cl. We shall show examples of the first attempt to examine the relationship between electron and ion temperatures (T_e and T_i) for individual plasma discharges. Our He-like spectra also exhibit effects of collisional coupling between metastable excited states. The collisional effects are density dependent and can be demonstrated in the present experiment because of the high and variable density ($\bar{n}_e \sim (0.5\text{-}8) \times 10^{14} cm^{-3}$) of the Alcator C tokamak.

The spectra of multi-electron systems are more complex, so the diagnostic use of these ions is only at a beginning. Initial identification of observed lines has begun with the help of calculated spectra. In the Alcator plasma, we find molybdenum in the charge states 28+ to 32+ which in itself is of interest for plasma fusion, since radiation from high Z multi-electron ions is an important loss factor to consider in the energy balance of the plasma [10]. The dominant features of the observed line emission from Mo have been identified with the principal 2p-3d transitions in Ne-like Mo^{32+} (this radiation was indicated by earlier measurements on Alcator A [11]. All together we have identified contributions from 2p-3d, 2p-3s, and 2s-3p transitions in Mo^{28+} to Mo^{32+} so that theoretical wavelengths can now be checked experimentally. Although the relative intensities of lines are presently

not theoretically well understood, the multitude of combinations of relative line intensities, which include principal and satellite lines of the same ion charge state as well as related lines in different charge states, suggests a rich source of information from TOXRASD of these data once the theoretical support is provided [12].

2. Experimental

2.1 Spectrometer Optics

The need to achieve high light collection efficiency dictates the use of a focussing spectrometer; the gain compared to a flat crystal is about two orders of magnitude [13]. Our spectrometer is based on the Van Hamos geometry [14]. It uses a cylindrically curved crystal where the focussing takes place in the vertical non-dispersive plane (see Fig. 1a). Despite the obvious merits of decoupling dispersion and focussing planes (for example, small optical aberrations), Rowland circle geometries have customarily been used for TOXRASD spectrometers [15,16]. In the Van Hamos geometry, a source point on the vertical plane through the cylinder axis is imaged on the same plane after the crystal. The incident photon flux is defined by a vertical slit so the angle of the diffracted photons is determined by Braggs law

$$\lambda = 2d \sin \theta \qquad (1)$$

The crystal length C (see Fig. 1b) defines the Bragg angle range to be

$$\Delta\theta_B = \frac{C}{L} \sin \theta_B = \frac{C}{\zeta} \sin^2 \theta_B \qquad (2)$$

where the radius of curvature is

$$\zeta = L \sin \theta_B \tag{3}$$

The bandwidth of the crystal can now be expressed as

$$\Delta\lambda/\lambda = \Delta E/E = (C/\zeta) \sin\theta_B \cos\theta_B \tag{4}$$

Our dimensions of ζ= 58.5 cm, C = 15 cm and $\theta_B = 33^o$ give $\Delta E/E$ = 12%. We note that for a central ray with $\theta = \theta_B$, the distance between the slit and crystal and between crystal and image is L = 106 cm while the distance between the slit and image is X_B = 177 cm. Finally we give the expression for the locus for the wavelength λ on the axis ℓ as

$$\ell = (X_B - X)\ \lambda/2d \frac{1}{\cos(\theta_B - \theta)} \simeq (X_B - X)\ \lambda/2d \tag{5}$$

with the dispersion determined by

$$d\ell/d\lambda = \frac{1}{2d}\left[X_B - X(\lambda)\right] + \left(\frac{2d}{\lambda}\right)^2 \frac{R}{d}\left[\left(\frac{2d}{\lambda}\right)^2 - 1\right]^{-1/2} \tag{6}$$

and hence $d\ell/d\lambda$= 0.29 mm/mR for $\theta = \theta_B$. The ℓ axis is perpendicular to the central ray $\theta = \theta_B$ and it defines the preferred orientation of the detector and the Bragg angle range of $\Delta\theta_B$ span the length $\Delta\ell$= 17 cm.

2.2 Crystal

For our application we needed a large area bendable crystal with high reflectivity. We thus chose a PET crystal which has a peak reflectivity of 80% with an integrated reflecting power of 2×10^{-4}. It could be made to the desired size of 10 x 15 cm and provides sufficient resolving power of $\Delta E/E \lesssim 1/5000$ from the 002 planes with a crystal spacing of 2d = 8.742 Å [17].

2.3 Detector

The ideal detector would be a large area position sensitive detector with good position resolution and high count rate capability. Lacking such an instrument at the outset of this experiment, we chose initially to use a commercially available soft X-ray detector which compromised many of the optical capabilities of the crystal. The initial measurements were done with a single wire proportional counter [18]. The active detector area is 100 x 6 mm and gives a maximum spatial resolution of about 180 μm at 5.9 keV which is estimated to be about 350 μm at 2.5 keV. The position is derived from the time difference between pulses reaching the two ends of the high resistivity carbon coated quartz wire. The signals are processed with standard electronics and the resulting position spectrum is stored in an MCA and then fed into a PDP/II computer. The count rate capability is about 20 KHz; higher rates adversely affect both resolution and live time. The TOXRASD results presented here were taken with this detector, which was remotely moveable to cover different segments of the spectrometer band width.

From these experiments it was realized that the key to improving accuracy and diagnostic power of TOXRASD measurements is broad band width; i.e., it was crucial to find a detector closer to the ideals set by the optical capabilities. To obtain good spatial resolution and high count rate capability we chose a proportional counter with a low impedance active delay line. The active delay line gives good spatial resolution in one direction, and the anode wire plane can be used for coarse position determination in the other direction. The pulses from this detector are very fast (rise time about 3 ns and widths about 8 ns) giving a count rate capability of a few MHz. With a small detector (30 x 30 cm^2) a spatial resolution of 80μm has been achieved at 5.9 keV and tests in the spectrometer have shown neglible line width contribution from the detector (or less than 200μm) [19]. Very recently, we have built a 25 cm long detector which will cover the practically useful spectrometer band width and preliminary tests indicate that also this detector will not contribute significantly to the widths of measured lines in the spectra [20]. The count rate capability is believed to be up to 1 MHz when using fast CAMAC electronics for time encoding and for histogramming. We thus envisage that TOXRASD, with proper instrumentation, can be used for detailed characterization of the time history of individual X-ray lines from single discharges.

2.4 Spectrometer System and Light Source

The spectrometer coupled to the Alcator C tokamak is shown in Fig. 2. The viewing aperture required is 78 and 94 mrad (horizontally and vertically) which is essentially the solid angle subtended by the crystal viewed from the slit. The slit is located about 60 cm from the plasma center and central line of sight is through the vertical center of the

plasma, which has a minor radius of 16 cm. In order to utilize the vertical imaging capability of the spectrometer, the source to slit distance would have to be decreased, which present access constraints do not permit. This, however, is not a major concern, since the vertical focussing provides the desired high light collection efficiency. Considering the added technical difficulties and the practical consequences of handling multi-parameter data at high rates, we feel that vertical imaging TOXRASD measurements should be done with a narrow band spectrometer as a complement to the broad-band instrument presented here.

Important factors for the performance of the spectrometer system are the light collection efficiency (e) as determined by the solid angle (s) for measuring individual X-ray lines, the transmission efficiency (t), and the slit area (a). The maximum count rate depends on the detector system as discussed above. The vertical acceptance angle is 94 mrad (as stated above) and the horizontal one is determined by the width of the line observed. A typical value for the width is 0.7 mm at the detector (but excluding the detector contribution) which corresponds to 0.7 mrad. Hence the solid angle for line measurements is $s \approx 6 \times 10^{-6}$ sr. The photon transmission efficiency is $t \approx 0.22$ determined by losses in the entrance window (0.077mm Be), detector window (0.13mm Be), and crystal reflectivity. The slit area is $a = 0.2 \times 6 = 1.2$ mm^2. This cross section, times the emitting plasma diameter (15 cm) gives a source volume of .180 cm^3. The brightness B in units of photons/sec.cm^2.sr is then determined by

$$B = \int \frac{\varepsilon(r)dr}{4\Pi} \qquad (7)$$

with the emissivity $\varepsilon(r)$ in units of photons/sec.cm^3 given as

$$\varepsilon = 4\pi I \ (0.22 \times 6 \times 10^{-6} \times 0.18)^{-1} = 5.3.10^{7} \ . \ I$$

I is here the total number of measured photons per second for the considered line. As an illustration we can take an observed count rate of $I \sim 10^4\ s^{-1}$ for the strongest line w in the He-like spectrum of S or Cl. For this line we estimate a brightness of 6.3×10^{11} photons/sec.cm^2.sr which corresponds to a chlorine impurity density of $9.10^8\ cm^{-3}$ in agreement with estimates from other measurements [11].

3. Results and Discussion

A number of X-ray spectra have been recorded for plasma conditions in the range T_e = 1-2 keV and n_e = 1-8 x 10^{14} cm^{-3}. The lower density bound is a practical one set by the increase of runaway electrons with decreasing density which floods our detector with hard X-rays. A useful feature is the strong density dependence of the molybdenum impurity, so the Mo-emission practically disappears for $\bar{n}_e$ >2 x $10^{14}cm^{-3}$ allowing the study of S and Cl almost free from interference from other radiation except for a low bremsstrahlung and recombination continuum.

3.1 Spectra of S and Cl

An example of a spectrum taken with three detector settings is shown in Fig. 3. Each partial spectrum represents a single discharge with plasma conditions favouring emission from S and Cl. From the left we see the He-like n=2 to n=1 spectrum of Cl, the H-like spectrum of S and the He-like spectrum of S. The fine-structure splitting of the $2P_{3/2,1/2}$ to $1S_{1/2}$ resonance is visible despite the compromised resolution at the end of the detector; see ref. 21 for more details about the H-like S spectrum. It is interesting to note that the n=3 to n=1 He-like S spectrum lies in the region around λ= 4.3 Å just outside our present bandwidth bounds, but will be included with new instrumentation so three components of the S spectrum can be measured.

In order to identify the He-like spectrum in detail, we choose a discharge with suitably high line emission recorded in the Cl region (Fig. 4). The dominant peaks are due to the resonance (w), the intercombination (x,y), and the forbidden lines (z) from the upper states 2^1P_1, $2^3P_{2,1}$ and 2^3S_1; conventional lettering [23] is used for

transitions. We also see three satellites. The line q comes from single excitation of the S^{13+} ground state, while lines r and k belong to doubly excited upper states which are populated through dielectronic recombination. The observed spectrum is in excellent agreement with the predicted wavelengths of Vainshtein [22] which is equally true for both Cl and S including the H-like part (see ref. 21 for details). The relative line intensities are determined by the prevailing plasma conditions through the rates of the atomic transition involved, i.e., a situation of partially known models and partially known input parameters.

As an illustration of the use of correlated information in our TOXRASD spectra, we show the measured width of the resonance line ($\Gamma_{1/2}$) vs the relative intensity w/k (Fig. 5). The latter ratio expresses essentially the population ratio of electron impact excitation over dielectronic recombination, i.e., approximately a $T_e^{1/2}$ dependence. From the line width we extract a Doppler broadening, which gives the ion temperature T_i. From the experimental data on $\Gamma_{1/2}$ vs w/k we thus deduce T_i vs T_e. These results are of interest for determining the thermal coupling between electrons and ions; an interesting phenomenon in tokamaks is that T_i appears lower than T_e even at high densities when equilibrium would be predicted to prevail. Alternatively, given the T_i/T_e ratio for a discharge from other diagnostics, information can be extracted to test the atomic transition rates involved. If one wishes to pursue the question of the w/k ratio and the theoretical calculations of dielectronic recombination rates, the T_e information needed can be taken from the measured relative intensity of the resonance transitions in the H-like and He-like spectra [21]. These represent just a few examples of possible combinations of measured quantities. They illustrate how parameter

correlations can be used to characterize the plasma, since the thermal conditions governing the atomic rates involved can be specified as a state of equilibrium or be in a state of departure from a certain (coronal) equilibrium.

At densities of 10^{14} cm^{-3}, we expect to see collisional coupling between the metastable $2^3P_{2,1}$ and 2^3S_1 states which should cause the line ratio R=z/(x+y) to decrease with increasing density. In the low density limit R is predicted to be 2.2 and 1.9 for S and Cl while at densities of 4 x $10^{14}cm^{-3}$ it should have decreased by some 50% which is encouragingly close to observed typical average R values [9,23,24]. With improved instrumentation, both the density dependence $R(n_e)$ and correlation z/w vs. (x+y)/w can be measured with high accuracy and hence allow a detailed study of metastable states and their collisional couplings.

Although the gross features of our He-like and H-like line spectra are largely understood, a few phenomena have been observed which are beyond present theoretical interpretations. As an example we chose the fine structure splitting of the intercombination transition x/y (see Fig. 4) which is predicted to be independent of plasma conditions. For certain discharges we observe ratios which significantly depart from the predicted ratios of 0.52 and 0.65 for S and Cl [24]. These variations in the x/y ratio tell us that there must be a population channel for the 2^3P state, the rates of which depend on J, and that the plasma parameter controlling these rates is a hidden one [24].

We have mentioned already that the plasma can be assumed to be in a state of equilibrium or depart in some specified way from this state. However, present in tokamak plasmas are also certain instabilities which are locally or temporally limited so the plasma can continue to survive. A well known phenomenon is the sawtooth instability occurring in the center of the plasma with a time period of the order 10 ms. Our measurements have indicated that the X-ray signal over a wavelength region $\Delta\lambda \sim 0.4$ mÅ shows intensity variation synchronous to the sawtooth variation (Fig. 6). It is clear that it is of great importance to diagnose these and other instabilities at the level of the time history of individual X-ray lines; i.e., time resolved spectroscopy which is within the capacity of the improved instrumentation. In the future we shall thus have an opportunity to study the characteristic X-ray emission and the underlying atomic processes under extreme and unusual plasma conditions.

3.2 Emission From Molybdenum

For the identification of the complex Mo spectra (see Fig. 7) we rely crucially on theoretical spectra obtained from the extensive calculations [12]. The main groups of lines in the Mo spectrum can thus be identified with $2p_{1/2}$-3d transitions in the region λ = 4.6 to 4.7 Å and $2p_{3/2}$-3d in the region 4.8 to 4.9 Å. These principal 2p-3d transitions dominate the Mo-spectrum with contributions from the charge states Mo^{28+} to Mo^{32+}. In addition we also see a few dielectronic recombination lines, examples being some of the peaks between 4.816 and 4.846 Å. In the region 4.98 to 5.22 Å we identify contributions from the transitions $2p_{3/2,1/2}$-$3s_{1/2}$ in Mo^{32+} (at λ = 4.982, 5.207, and 5.217 Å) with some smaller contributions from the charge states Mo^{29+} to Mo^{31+}. Certain peaks like those at 5.155 and 5.163 Å have not yet

been assigned theoretical counterparts. Most transitions are of the dipole type while the 5.207 Å line is an example of magnetic quadrupole.

Finally, the region 4.41 to 4.50 Å contains some rather weak lines that have been attributed to 2s–3p transitions. From the above outline of the line identification of the observed Mo-spectrum (for a more detailed discussion of theory and experimental identification see ref. 12) it suffices to call attention to two results of these measurements. We have located the groups of lines separated by the spin-orbit splitting. Theory predicts this splitting qualitatively correctly but the spin-orbit strength, which gives the best overall wavelength agreement with the data, turns out systematically to overshoot the splitting for each type of transition. The other new finding is that the charge state abundance distribution is observed to be quite different from the one predicted assuming a plasma in coronal equilibrium. Our results, therefore, suggest either that the normal equilibrium assumption must be strongly violated (because of transport effects, for instance) or that the ionization rates used to calculate the abundance distribution need to be revised. For instance, the Mo^{32+} is calculated to be the dominant charge state at T_e ~3 keV which is not compatible with the relative line emission of Mo^{28+} to Mo^{32+} as measured at T_e = 1.2–1.6 keV [12,25].

4. Conclusion

We have reported on an experiment to measure soft X-ray line emission from highly ionized S, Cl, and Mo atoms in the hot plasma of the Alcator C tokamak. The aim of this project is to provide crucial diagnostics of the plasma in the endeavor towards achieving fusion conditions. The instrument developed for these measurements was described as well as the work to

optimize the spectrometer performance with regard to the broad-band time-resolved spectroscopy measurements. A crucial element for such measurements is the position sensitive X-ray detector. The design of such a detector was described which matches the optical capacity of the Van Hamos geometry used. Results from initial measurements of H- and He-like spectra for S and Cl were presented with diagnostic inferences drawn from the data. New spectroscopic information was also presented for the molybdenum spectrum in charge states between Mo^{28+} to Mo^{32+}. These charge states appear at temperatures of 1.2 to 1.7 keV which is some 50% below the predicted temperature of maximum abundance for Mo^{32+}. A unique feature of the present experiment is the high light collection efficiency which has allowed the first X-ray diagnostic of individual plasma discharges to be performed. With the new matching high resolution, high count rate detector system we envision the measurement of high accuracy, time-resolved spectra and hence the first impurity X-ray probing of the microscopic time variation of individual plasma discharges.

5. Acknowledgements

We are grateful to R. Parker and the Alcator group for the excellent support and interest in this diagnostics project. This work was supported by the U.S. Department of Energy and by the National Science Foundation. Support to one of us (EK) from Smithsonian Institution Fluid Research Funds is gratefully acknowledged.

REFERENCES

1. R. Giacconi and H. Tananbaum, Science 209, 865 (1980).
2. C. de Michelis and M. Mattioli, Nuclear Fusion 21, 677 (1981).
3. F. Folkmann et al., Nucl.Instr.Meth. 181, 99 (1981) and this volume.
4. B. Edlen, this volume.
5. S. Fairfax, et al., in Plasma Physics and Controlled Nuclear Fusion Research, Proc. 8th Int. conf., Brussels (1980) Vol. I, IAEA Vienna (1981) p439.
6. E.S. Marmar, et al., Nuclear Fusion 19, 485 (1979).
7. A. Gondhalekar et al., Journ.Magn.Materials 11, 359 (1979).
8. A.H. Gabriel and C. Jordan in Case Studies in Atomic Collision Physics, Vol. 2, Amsterdam, Holland (1971) p.211, and F. Bely-Dubau et al., Mon.Not.R.Astr.Soc. 198. 239 (1982).
9. A.K. Pradhan and J.M. Shull, Astroph.Journ. 249, 821 (1981).
10. H.P. Summers and R.W.P. McWhirter, J.Phys.B 12, 2387 (1979), and H.W. Drawin, Physica Scripta 24, 521 (1981).
11. J.E. Rice, et al., Phys. Rev. A22, 310(1980).
12. E. Källne, J. Källne, and R.D. Cowan, to be published (1982) and R.D. Cowan, this volume.
13. B. Yaakobi, R.E. Turner, H.W. Schnopper, and P.O. Taylor, Rev.Sci.Instr., 50, 1609 (1979).
14. L. Van Hamos, Arkiv for Mat.Astr.Fys., 31A, 1 (1945), and C.B. van den Berg and H. Brinkman, Physica XXI, 85 (1955), and H.W. Schnopper and P.O. Taylor, DOE Report E4-76-S-02-4021, 1977.
15. K.W. Hill, et al., Phys.Rev. A19, 1970 (1979).
16. P. Platz, et al., Ass.Euratom EUR-CEA-FC-1057, June 1980.

17. A. Burek, Space Science Instrum. 2, 53 (1976), N.G. Alexandropoulos and C.G. Cohen, Appl.Spectr. 28, 155 (1974), and R. Hall, et al., Univ. Leicester Report, Jan. 1978.

18. C.J. Borkowski and M.K. Kopp, Rev.Sci.Instr. 46, 951 (1975), and TEC Model 210, Technology for Energy Corp., Knoxville, Tenn. 37922, USA.

19. J. Källne, E. Källne, L.G. Atencio, C.L. Morris, and A.C. Thompson, Nucl.Instr.Meth., to appear (1982).

20. J. Källne, et al., Fourth Topical Conf. on High Temperature Plasma Diagnostics, Boston, Aug. 1982, Bull. Am. Phys. Soc. (1982).

21. E. Källne, J. Källne, and J.E. Rice, Phys.Rev.Letter, 49,330, 1982.

22. L.A. Vainshtein and U.I. Safronova, Atomic Data and Nuclear Data Tables 21, 49 (1978).

23. C.P. Bhalla, A.H. Gabriel, and L.P. Presnyakov, Mon.Not.R.Ast. Soc., 172, 359 (1975).

24. E. Källne, J. Källne, and A.K. Pradhan, submitted for publication (1982).

25. C. Breton, et al., Association Euratom CEA, EUR-CEA-FC-948, March 1978.

FIGURE CAPTIONS

Fig. 1 a) Schematics of the dispersive and focussing properties of the cylindrically bent crystal in the used spectrometer geometry of Van Hamos. b) Definition of the main optics parameters.

Fig. 2 a) Photograph of the spectrmeter at the Alcator C tokamak; the white dewar and the 16'' vacuum ports of the tokamak are visible. b) Layout of the spectrometer at Alcator C.

Fig. 3 Example of the line emission from sulphur and chlorine observed in the wavelength region 4.3-5.3 Å; for line identification see the text. The spectrum is composed of three recordings of individual discharges with the detector appropriately re-positioned between the shots. The plasma conditions were $\bar{n}_e = 2.9 \times 10^{14} cm^{-3}$ and $T_e \sim 1.1$ keV.

Fig. 4 Example of spectrum recorded for a single plasma discharge showing strong line emission from He-like (lines w,x,y, and z) and Li-like (lines q,r, and k) chlorine. Plasma parameters for this shot were $\bar{n}_e = 2.3 \times 10^{14}$, $T_e = 1.4$ keV. The spectrum was recorded during a 200 msec timegate.

Fig. 5 Line widths of the (w) resonance line (T_i) plotted vs. the line intensity ratio w/k (T_e) determined for single discharges. The solid line shows the locii of $T_i=T_e$. The points falling far below the main ensemble of data (marked with x) belongs to discharges that terminated in disruptions.

Fig. 6 Typical temporal behaviour of a plasma shot showing the following parameters (from top to bottom): electron density (0.58 x $10^{14}cm^{-3}$/fringe), plasma current (375 kA at peak), central soft X-ray emission ($E_{h\nu}$ >1 keV), and TOXRASD at 4.6 to 4.9 Å. The two lower traces show a temporal expansion of the soft X-ray and TOXRASD and the sawtecth oscillations.

Fig. 7 Spectrum composed of three detector settings showing the line emission over the full range of the spectrometer acceptance (λ = 4.3-5.3 Å). Emission from S^{14+}, S^{15+}, Cl^{15+}, Mo^{30+}, Mo^{31+}, and Mo^{32+} is seen. The low electron density $\bar{n}_e = 1.5 \times 10^{14}cm^{-3}$ and high temperature T_e ~1.4 keV for these plasma shots enhances the Mo emission over that of S and Cl.

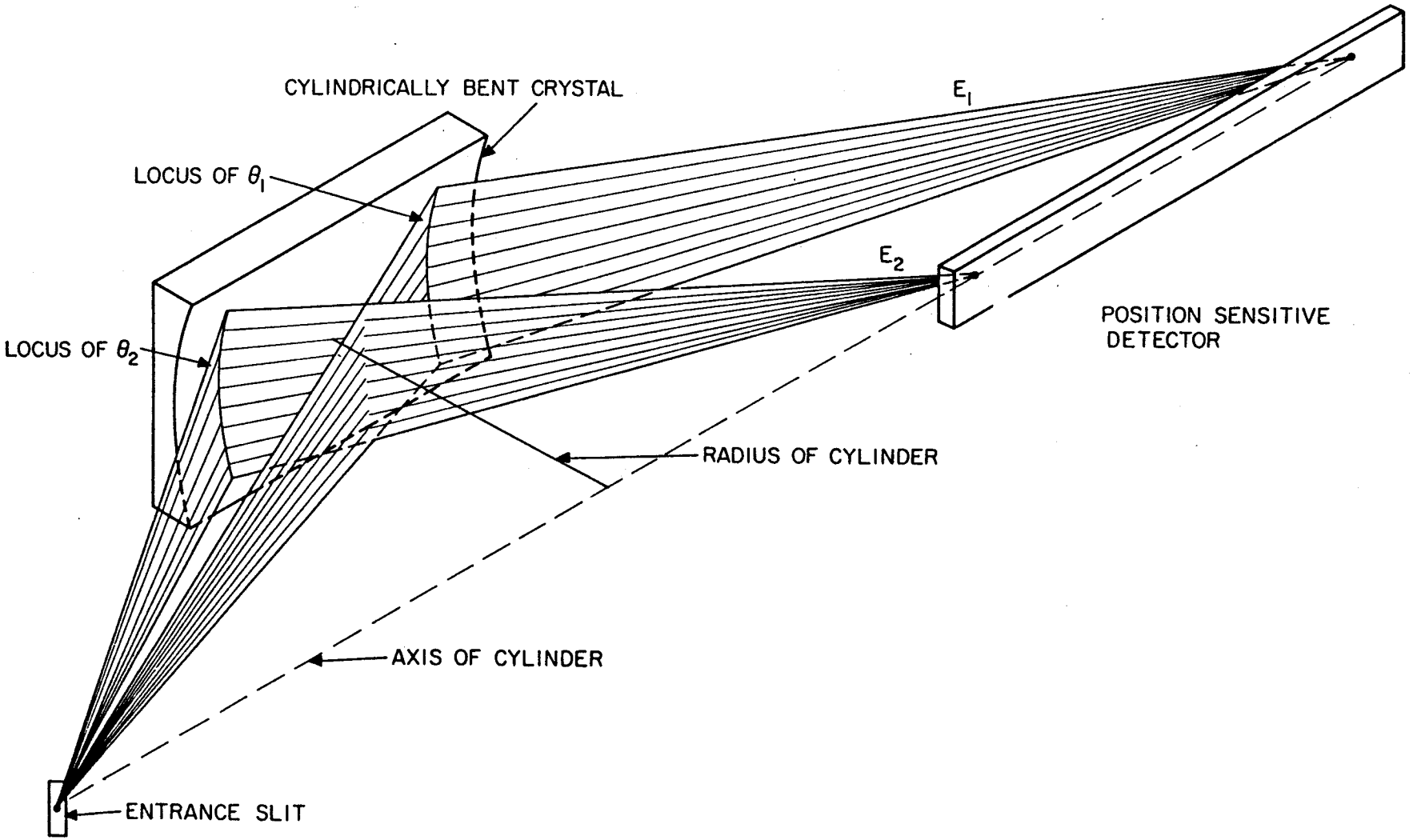
CYLINDRICALLY BENT CRYSTAL
E_1
LOCUS OF θ_1
E_2
POSITION SENSITIVE DETECTOR
LOCUS OF θ_2
RADIUS OF CYLINDER
AXIS OF CYLINDER
ENTRANCE SLIT

Fig.1a

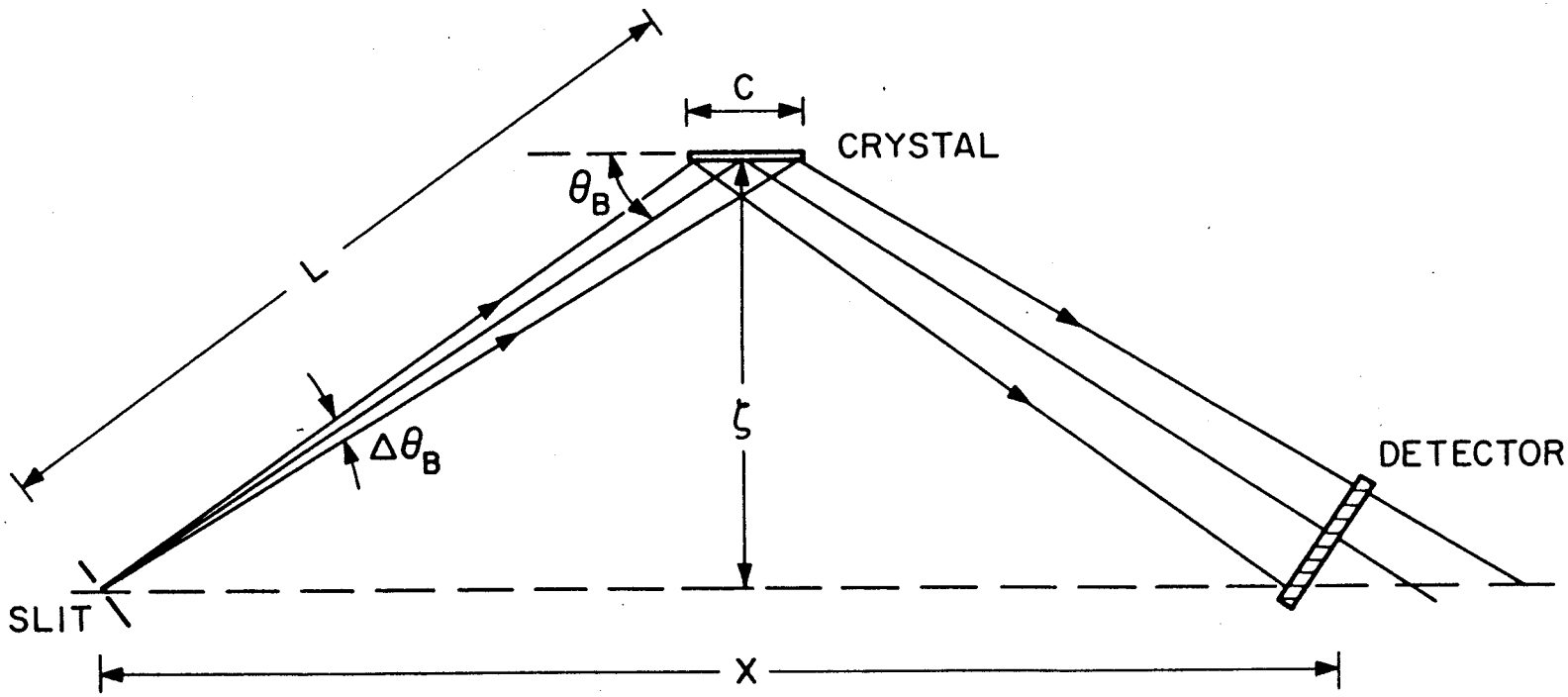

Fig.1b

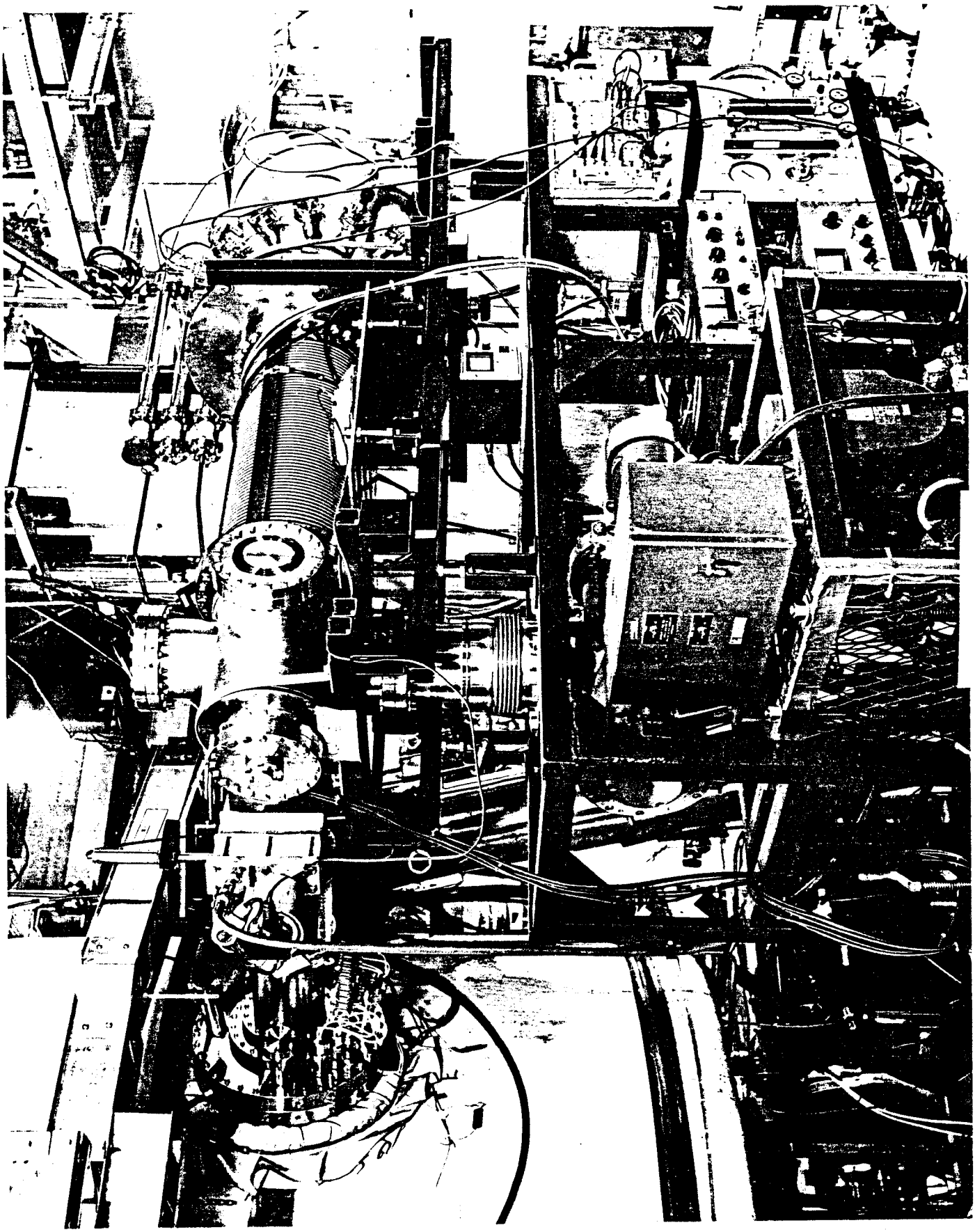

Fig.2a

HIGH RESOLUTION CRYSTAL SPECTROMETER AT ALCATOR C

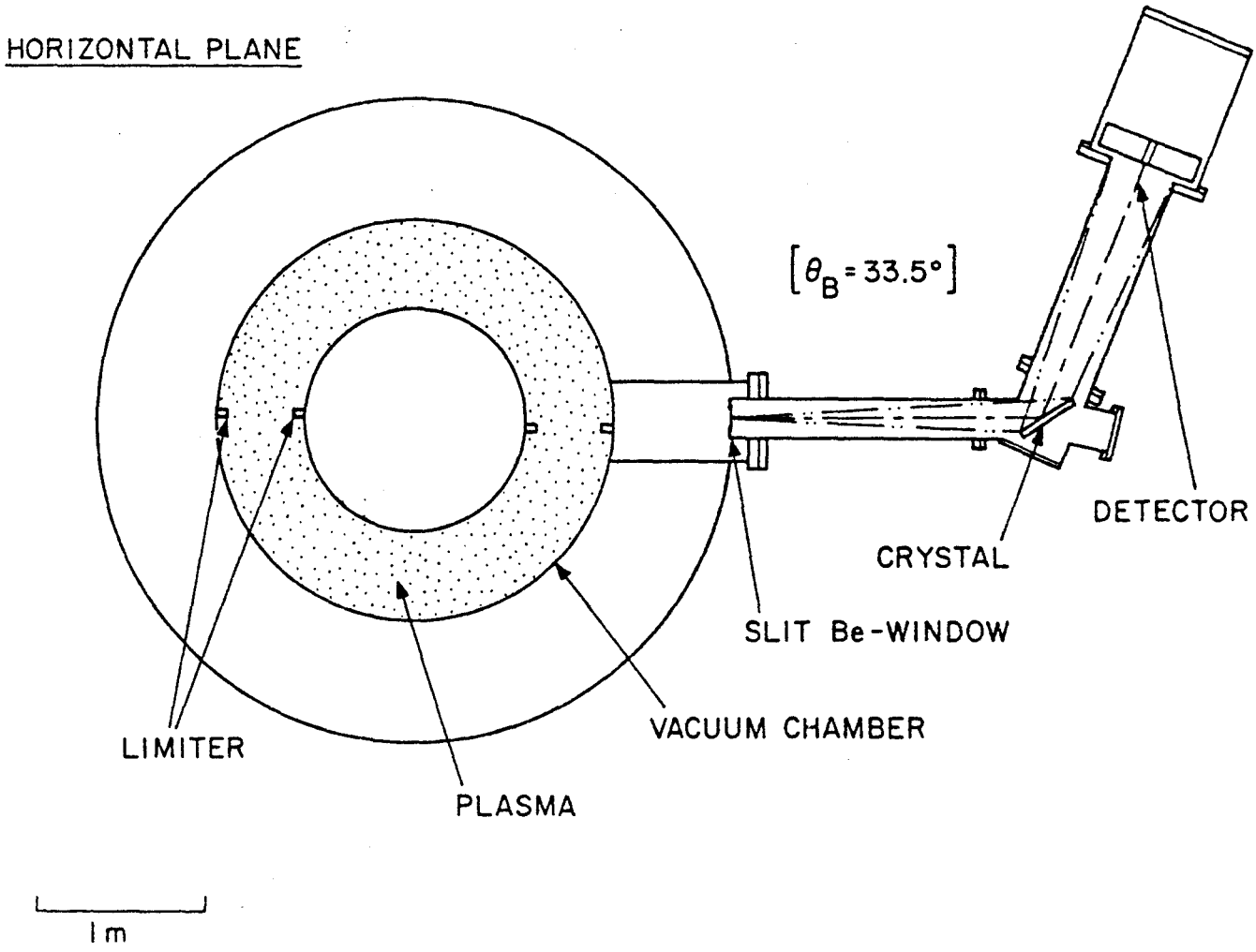

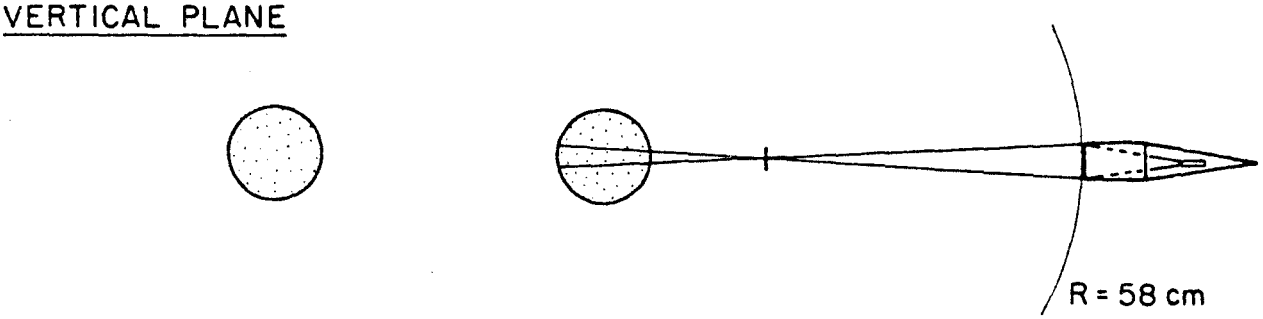

Fig.2b

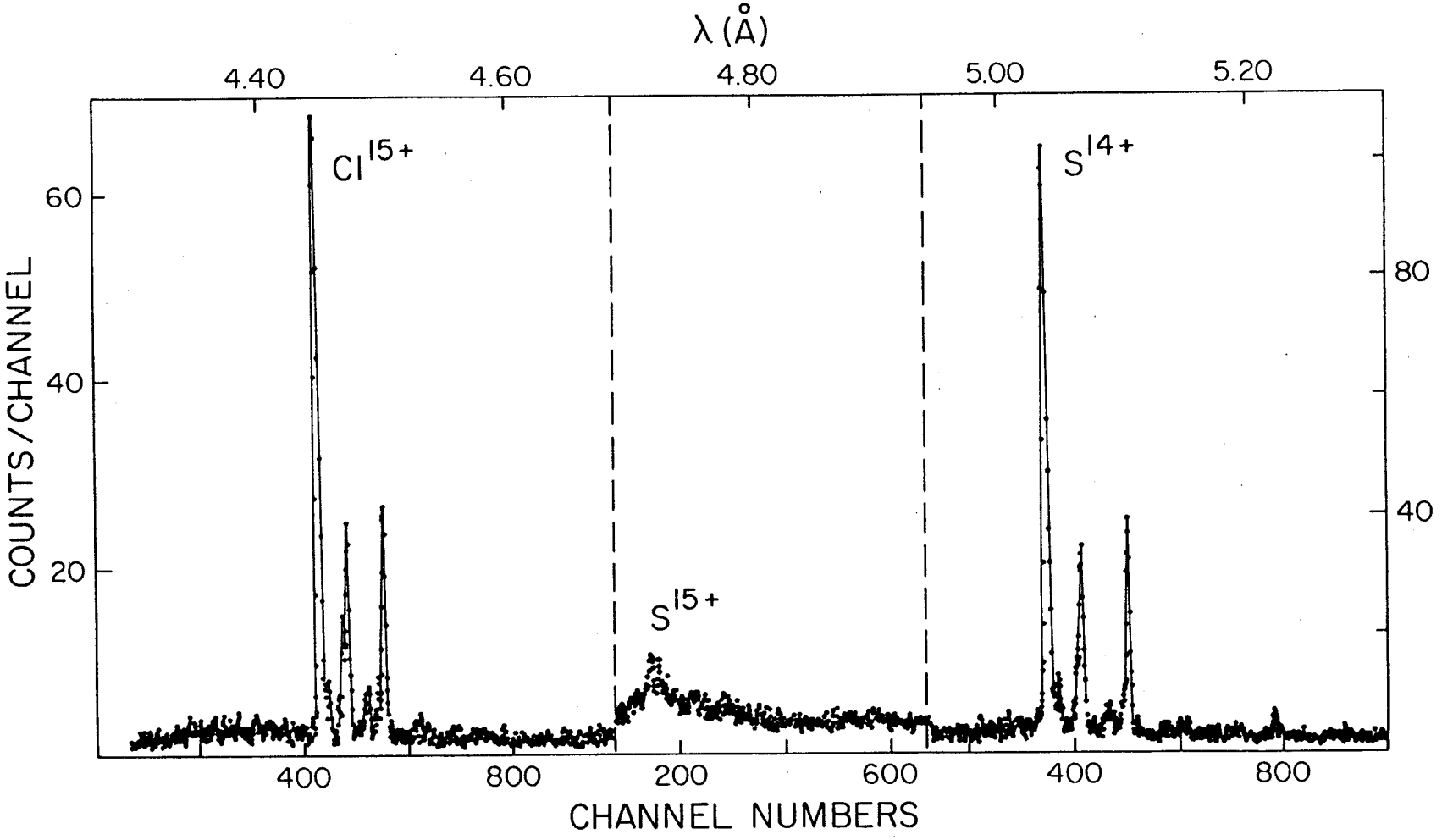
λ (Å)
4.40
4.60
4.80
5.00
5.20
Cl15+
S15+
S14+
60
40
20
80
40
COUNTS/CHANNEL
400
800
200
600
400
800
CHANNEL NUMBERS

Fig.3

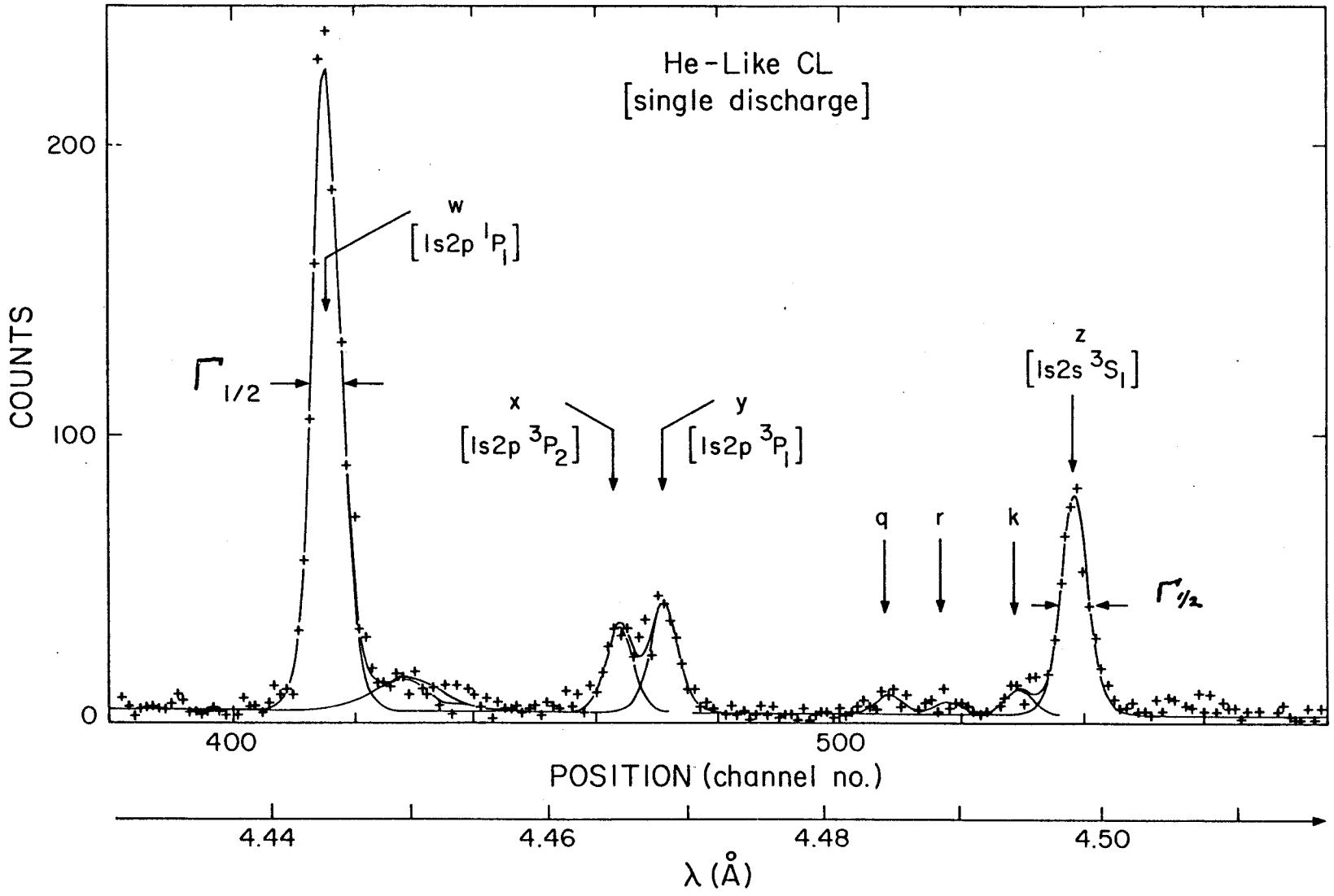
He-Like Cl
[single discharge]
COUNTS
200
100
0
w
[1s2p $^1P_1$]
$\Gamma_{1/2}$
x
[1s2p $^3P_2$]
y
[1s2p $^3P_1$]
z
[1s2s $^3S_1$]
q
r
k
$\Gamma_{1/2}$
400
500
POSITION (channel no.)
4.44
4.46
4.48
4.50
λ (Å)

Fig.4

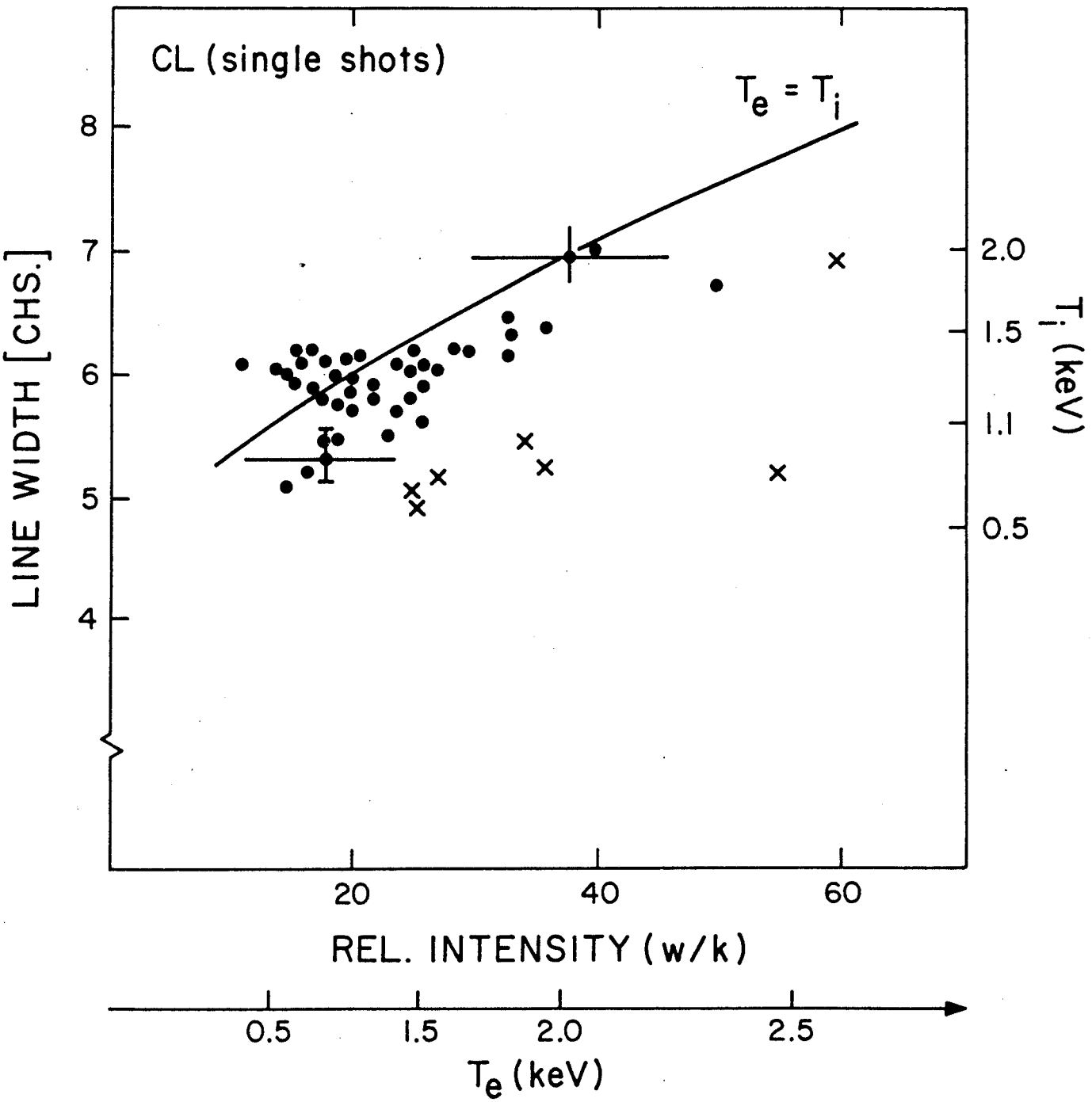
CL (single shots)
$T_e = T_i$
LINE WIDTH [CHS.]
8
7
6
5
4
T_i (keV)
2.0
1.5
1.1
0.5
20
40
60
REL. INTENSITY (w/k)
0.5
1.5
2.0
2.5
T_e (keV)

Fig.5

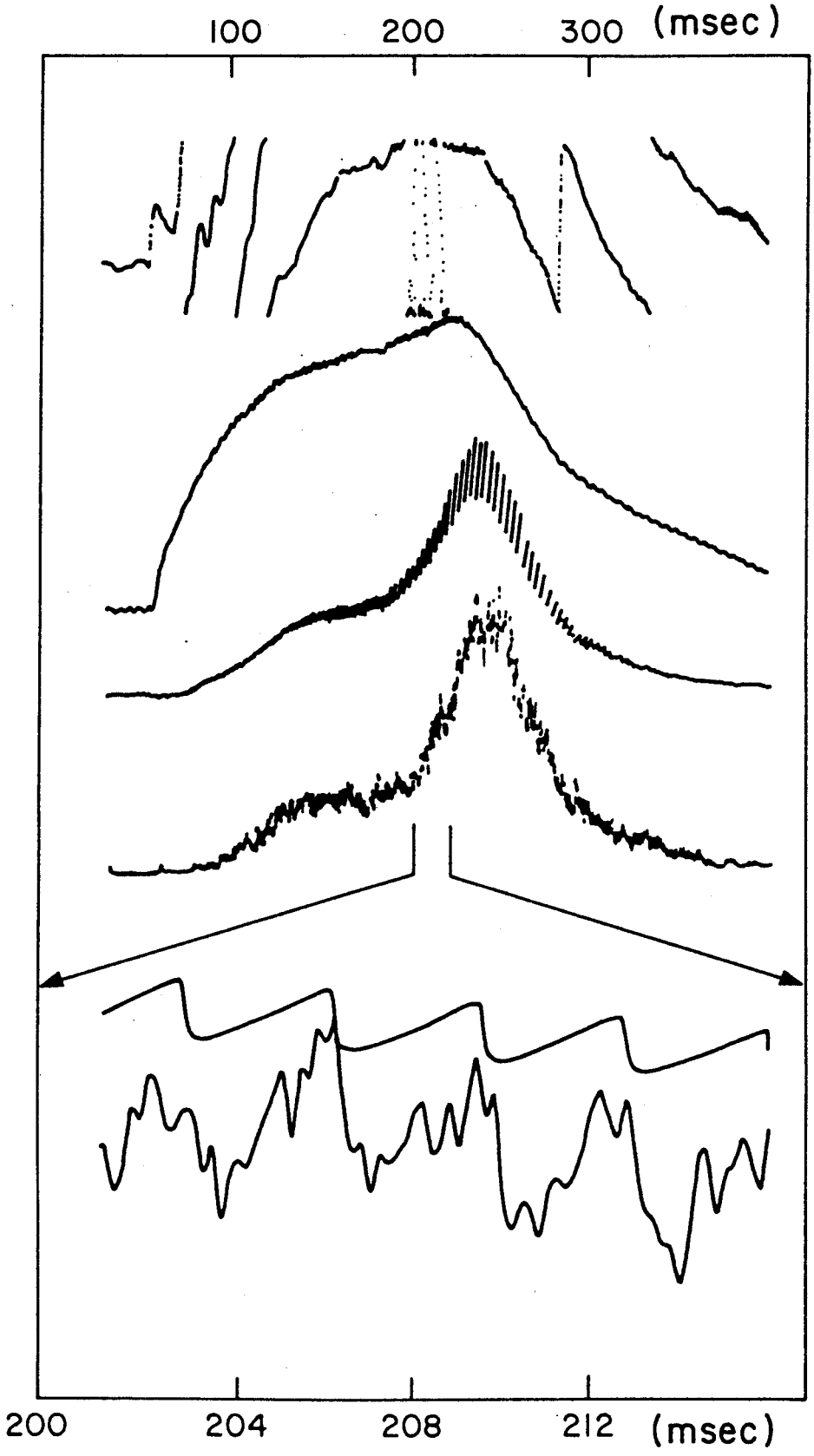

Fig.6

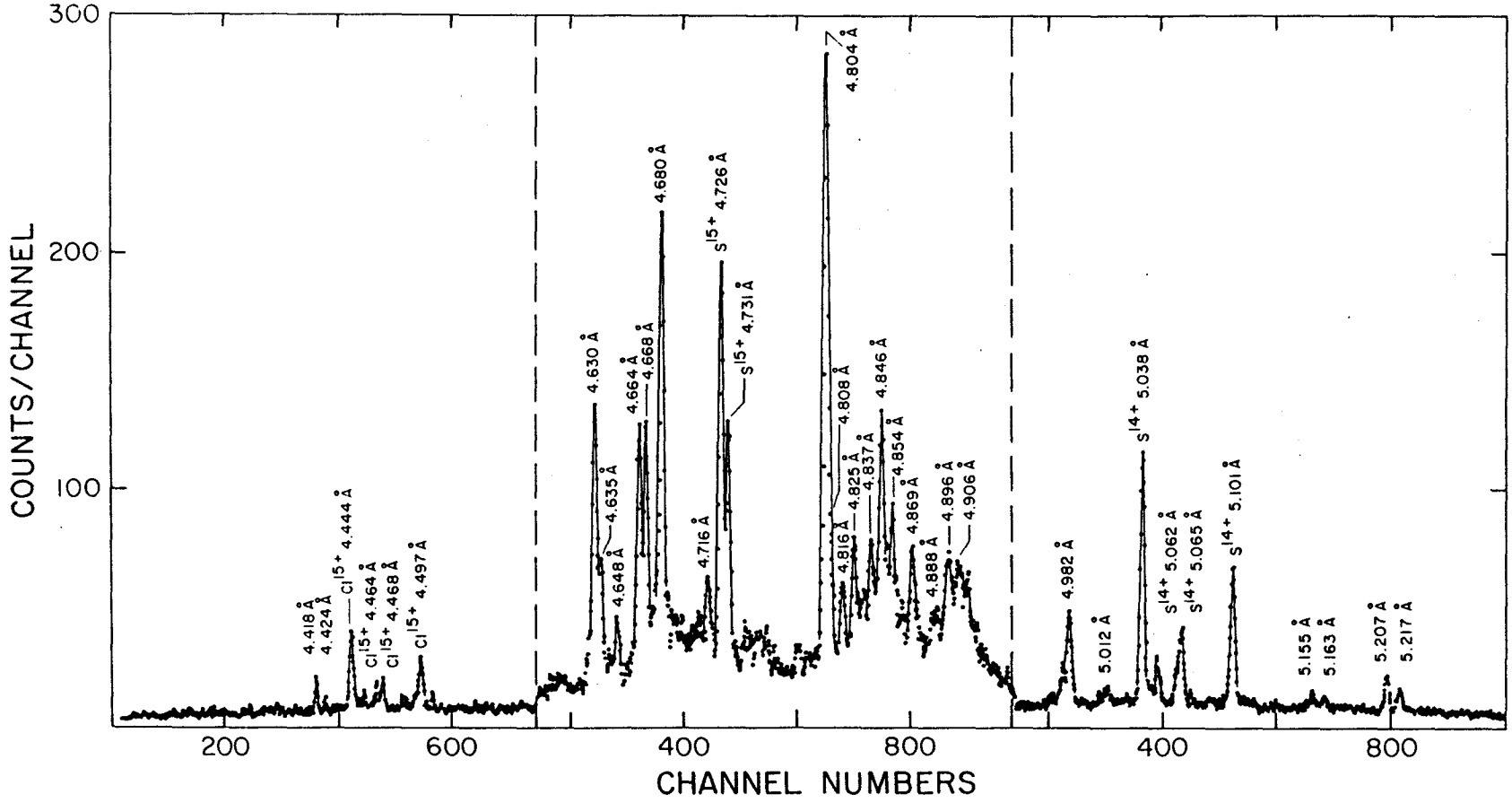
COUNTS/CHANNEL
300
200
100
200
600
400
800
400
800
CHANNEL NUMBERS
4.418 Å
4.424 Å
Cl15+ 4.444 Å
Cl15+ 4.464 Å
Cl15+ 4.468 Å
Cl15+ 4.497 Å
4.630 Å
4.635 Å
4.648 Å
4.664 Å
4.668 Å
4.680 Å
4.716 Å
S15+ 4.726 Å
S15+ 4.731 Å
4.804 Å
4.808 Å
4.816 Å
4.825 Å
4.837 Å
4.846 Å
4.854 Å
4.869 Å
4.888 Å
4.896 Å
4.906 Å
4.982 Å
5.012 Å
S14+ 5.038 Å
S14+ 5.062 Å
S14+ 5.065 Å
S14+ 5.101 Å
5.155 Å
5.163 Å
5.207 Å
5.217 Å

Fig.7